

Excitation of Rydberg wave packets with chirped laser pulses

J. Preclík¹, M. Kozák², D. Fregenal³, Ø. Frette¹, B. Hamre¹, B. T. Hjertaker¹, J. P. Hansen¹, and L. Kocbach¹

¹*Department of Physics and Technology, University of Bergen, N-5007 Bergen, Norway*

²*Faculty of Mathematics and Physics, Charles University in Prague, Ke Karlovu 3, 121 16 Prague 2, Czech Republic*

³*Centro Atómico Bariloche and Consejo Nacional de Investigaciones Científicas y Técnicas, R8402AGP San Carlos de Bariloche, Argentina*

(Received 20 September 2012; revised manuscript received 20 November 2012; published 26 December 2012)

We study Rydberg wave packets produced by pairs of time separated femtosecond laser pulses. The time separation ranges from femtosecond to picosecond time scales. The wave packets consist predominantly of f states of principal quantum numbers $n = 22\text{--}32$ in Li. With a direct analysis of the field ionization spectra the n -level-resolved classical orbit times are displayed. By chirping the second excitation pulse we demonstrate controlled amplitude oscillations of n -level amplitudes on femtosecond time scales.

DOI: [10.1103/PhysRevA.86.063418](https://doi.org/10.1103/PhysRevA.86.063418)

PACS number(s): 32.80.Rm, 32.80.Ee, 82.53.Hn

I. INTRODUCTION

The concept of wave packets consisting of a superposition of atomic Rydberg levels excited by short laser pulses is more than 25 years old [1]. Wave packets are quantum states which may be well localized in space, and their investigation on both theoretical and experimental sides contributes to understanding the transition between classical and quantum physics. From an applied point of view, the controlled manipulation of Rydberg states is important for quantum information.

The generation and detection of the atomic Rydberg wave packets was first proposed by Alber *et al.* [1]. Since then, extensive experimental studies have followed in parallel with the development of the ultrafast laser technology, from the picosecond to the femtosecond time regimes. The first experimental study of the radially localized Rydberg wave packets was realized in 1988 by ten Wolde *et al.* [2], where the dynamics of the rubidium Rydberg wave packet was investigated in a pump-probe experiment. This pump-probe method, with the detection of the photoionized electrons, was subsequently used in the study of wave-packet dynamics in external electric fields [3,4]. The next improvement in this setup took advantage of different wavelengths [5,6]. Phase-sensitive detection was also demonstrated [7] when the exciting laser light was modulated and the resulting ion signal was bandpass filtered. This method enabled precise measurements of the Rydberg wave-packet dynamics in electromagnetic fields and in fields above the ionization limit [8–10].

A new method, so-called Ramsey optical spectroscopy, for studying the Rydberg wave packet dynamics was proposed by Noordam *et al.* [11]. In this technique the final population of atomic Rydberg states after an excitation with a pair of short optical pulses is determined by the selective field ionization method (SFI). Ramsey fringes spectroscopy requires the control of the delay between the two excitation pulses on a subfemtosecond time scale in order to manipulate the phase difference between the incident fields. In this setting the atomic system exhibits oscillations in two different time domains: (i) fast oscillations at optical frequencies and (ii) modulations on a slower time scale characterizing the wave-packet dynamics. Experimentally this method was used to study the wave-packet dynamics in strongly driven Rydberg atomic systems [12] including also a three-pulse version of the experiment [13] and studies of macroscopically distinct states [14].

In parallel, theoretical improvements of the Ramsey atomic interferometry method were suggested. First, the realization of cross-correlation interferograms with two different optical pulses (e.g., one Fourier-transform limited and second chirped) could provide additional information about the lifetimes of excited states [15]. Second, the evolution of Ramsey fringes after multiple-pulse excitation and engineering of tailored wave packets was explored [16,17]. Finally, a Fourier transform method, to establish phases and amplitudes for each Rydberg n -level up to a global (unimportant) phase, based on time series of state probabilities was developed [18]. Recently, this method has been applied in determining the amplitudes of ionic Rydberg wave packets [19].

With the exploration of phase-controlled femtosecond laser pulses, laser excitation of Rydberg wave packets gained a new dimension: Cross-correlation interferograms with shaped pulses and programmable wave packets were demonstrated [20]. A method to determine the phase and amplitude of a quantum wave packet based on analysis of covariant fluctuations was introduced [21], followed by the experimental excitation of a desired wave packet by shaped femtosecond laser pulses, which were computer controlled in an iterative feedback loop [22]. Finally, information storage and retrieval through quantum phases of Rydberg wave packets were demonstrated by Ahn *et al.* in 2000 [23]. Despite the large number of experimental studies, the number of direct displays and analysis of raw experimental data from atomic Ramsey fringes experiments are rather few. In particular the resolution of individual n -level dynamics has not been given much attention previously. An exception is the more recent work of Carley *et al.* [24] in which wave-packet dynamics in Na (ns and nd) is studied.

In this work we study Rydberg wave packets produced by pairs of time-separated femtosecond laser pulses exciting Li($3d$) atoms. The SFI spectrum obtained for each time delay between the pulses is placed at the corresponding position in a two-dimensional map where one direction is the SFI time and the other is the delay time. The resulting maps of SFI spectra are then further analyzed as a function of the delay time. We thus present a direct n -resolved experimental observation of cross-correlated interferograms of the atomic Rydberg wave packets realized with either a pair of Fourier-transform-limited pulses or a pair where one is a chirped laser pulse. The measurements are compared with a straightforward

perturbation theory analysis. The time separation ranges from femtosecond to picosecond time scales. On the picosecond time separation the classical orbit times are displayed and on femtosecond time scales, using a linearly chirped second pulse, we demonstrate controlled amplitude oscillations.

The paper is organized as follows. In the next section the experiment is described, followed by a section describing the applied theoretical model. Finally, in Sec. IV we present and discuss our results. Atomic units are used unless explicitly mentioned otherwise.

II. EXPERIMENTAL DETAILS

A collimated thermal beam of lithium atoms was prepared in the vacuum chamber ($<10^{-6}$ mbar) by heating metallic lithium to ≈ 400 °C in an oven with a narrow exit channel. The size of the beam in the excitation region was $2\text{ mm} \times 10\text{ mm}$ and the average speed of atoms was $1.43\text{ mm}/\mu\text{s}$. The laser excitation and the SFI detection were realized in the same region.

The lithium atoms were excited from the ground state to the $3d$ state by the sequence of two dye laser pulses with wavelengths 611 nm ($2s \rightarrow 2p$) and 671 nm ($2p \rightarrow 3d$). The dye lasers were pumped with the second harmonics of the Nd:YAG laser (pulse duration, 5 ns ; repetition rate, 14 Hz ; wavelength, 532 nm). The 140-fs pulses generated in the tunable femtosecond oscillator (Chameleon Ultra II, Coherent, 80 MHz ; average power, 3 W) were used for excitation from $3d$ to superposition of nf Rydberg states ($n > 19$). The contribution of the np states to the total superposition is estimated to be about 3% from the comparison of the dipole transition elements.

The lifetime of electrons in the $3d$ state of lithium is approximately 14 ns , while the time delay between the following femtosecond pulses is 12.5 ns . This means that the Rydberg wave packet was excited only with one femtosecond pulse immediately following the dye laser nanosecond excitation. As the original output from the femtosecond laser was too weak to have good signal-to-noise ratio, we amplified this femtosecond pulse in the dye cell pumped with a part of the energy of Nd:YAG laser. This allowed us to both increase the probability of excitation and synchronize the strong pulse with the excitation pair of nanosecond dye laser pulses. We used the solution of the laser dye LDS 821 in methanol with a concentration of 40 mg/l . The spectral window of the optical gain was $820\text{--}840\text{ nm}$. The amplified pulse energy depended on the time overlap of the nanosecond pump pulse with the femtosecond pulse. We reached an average energy of the amplified pulse as high as $4\text{ }\mu\text{J}$ (the initial pulse energy of the femtosecond laser was 30 nJ).

For the time-resolved experiments, the Michelson interferometer was used to prepare a pair of coherent femtosecond pulses with a variable time delay (see Fig. 1). A computer-controlled linear stage with a minimal step of 5 nm was used for this purpose. For the cross-correlation interferometry experiment with a chirped pulse, a pulse stretcher consisting of two prisms was added into one arm of the Michelson interferometer. The resulting pulse was down-chirped (higher frequencies arrive sooner than lower frequencies) with a total length of about 300 fs (see Fig. 2). The stretcher was able

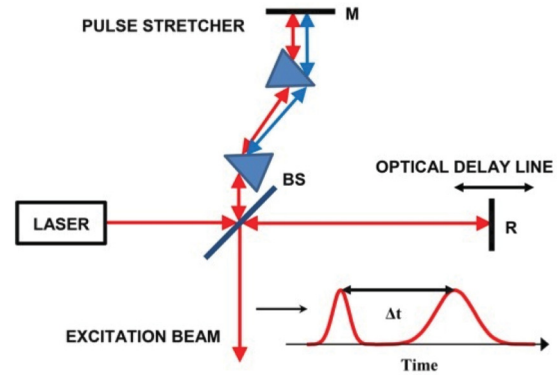


FIG. 1. (Color online) Experimental setup for cross-correlated interferogram measurements. M, mirror; BS, beam splitter; R, retroreflector.

to chirp the pulse up to 5000 fs^2 depending on the distance between the prisms.

The femtosecond laser pulses were characterized using the frequency-resolved optical gating method implemented in a commercial setup using the Grenouille 8-50 (Swamp optics) and their parameters were retrieved by the commercial software Femtosec Technology QuickFROG. The dye cell amplifier stretched the pulses up to 150 fs (see Fig. 2). The pulse characterization was done with nonamplified pulses. The amplified pulses were also characterized using synchronized triggering with the Nd:YAG laser. The shape and the length of the pulse did not significantly differ from the unamplified pulse which went through the dye cell without Nd:YAG pumping (cf. Fig. 2). Any possible difference will not influence the results of

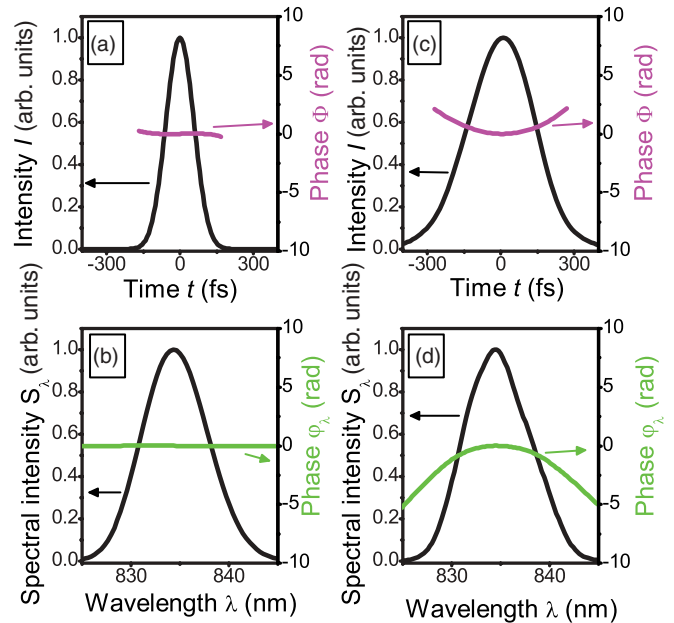


FIG. 2. (Color online) Retrieved characterization of the used femtosecond laser pulses from FROG measurements. (a) Time profile and temporal phase of the Fourier-transform-limited pulse. (b) Spectrum and spectral phase of the Fourier-transform-limited pulse. (c) Time profile and temporal phase of the down-chirped pulse, (d) Spectrum and spectral phase of the down-chirped pulse.

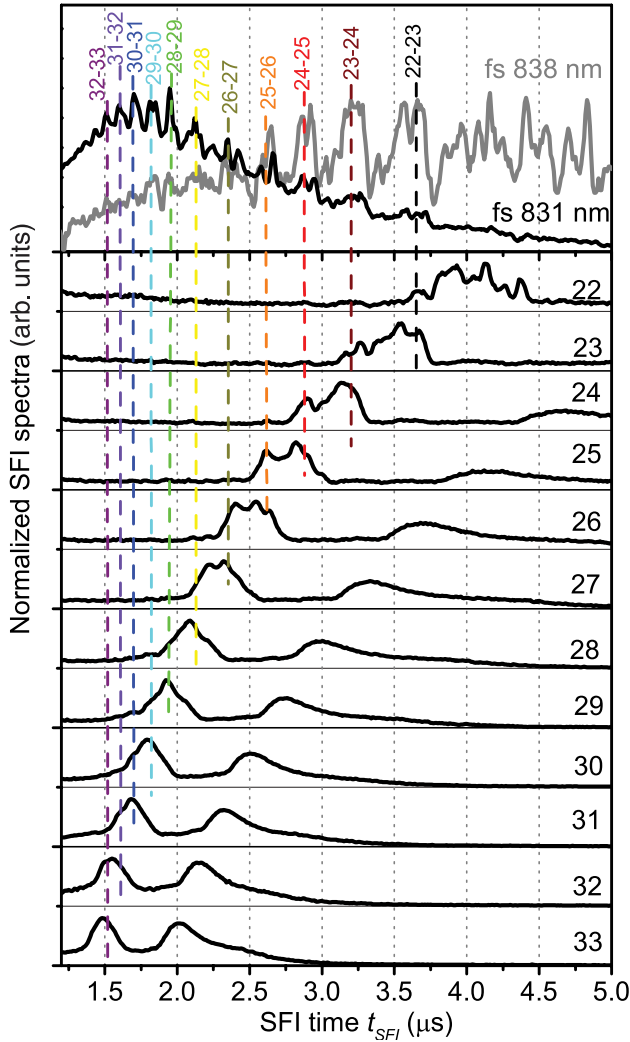


FIG. 3. (Color online) SFI signals. Upper thick lines: SFI spectra of atoms excited to superposition of Rydberg states by femtosecond laser pulses with central wavelengths of 831 and 838 nm. Lower lines: SFI spectra of $n = 22$ to $n = 33$ f states excited individually by tunable nanosecond laser pulses with narrow spectral bandwidth. The vertical lines indicate the values of t_{SFI} used in the state resolution analysis in Figs. 5–7.

the interferometric measurements as the only crucial parameter is the relative phase shift between the pulses produced in the interferometer, which will be the same for all incoming pulses.

The Rydberg states were detected by the SFI technique. For this purpose, a linear voltage ramp [25] was applied. It created an electric ramping field \mathbf{E}_{SFI} with a slew rate of $E_{\text{SFI}} \simeq 500$ V/cm/ μs . This field \mathbf{E}_{SFI} selectively ionizes different Rydberg states at different instants of time t_{SFI} and accelerates the resulting Li^+ ions onto a channeltron detector operating in proportional mode. The signal is registered by a digital oscilloscope. In the presented measurements the registered spectra (as shown in Fig. 3) result from accumulation of the signals from 1000 repeated laser flashes. This part of the experimental arrangement, the timing of the components and the SFI data collection procedure have been developed and described in a series of our studies of Rydberg atom processes (e.g., Refs. [26,27]).

In this region of the experimental setup a small constant electric field was applied to suppress signal caused by spurious ions produced by multiphoton ionization or induced by collisions, without producing l mixing. In order to identify contributions from individual nf levels in the SFI spectra the femtosecond laser pulses were also replaced by the output from a tunable commercial nanosecond dye laser (Quantel, TDLIII) with a narrow bandwidth, which to a high degree of accuracy excites only the individual levels. These individual-level SFI spectra for $n = 22$ to $n = 33$ are compared with the SFI spectra of atoms excited by the femtosecond pulses in Fig. 3, thus effectively calibrating the SFI arrangement for resolution of individual n levels. The vacuum chamber is cooled to liquid nitrogen temperature in order to minimize the effect of blackbody radiation.

The SFI spectra of superpositions of Rydberg nf states after femtosecond laser excitation have the following features: The first peak, arriving into the detector at $t_{\text{SFI}} = 1$ μs , (not shown in Fig. 3) is caused by arrival of free ions present in the chamber prior to the SFI voltage rise. These ions originate mostly from a parasitic effect: three-photon ionization of lithium atoms driven by the dye lasers. A typical spectrum of a single nf state consists of two main peaks, which can show further more complicated structure. The first adiabatic peak that occurs at lower ionization voltages corresponds to the ionization of states with low values of the magnetic quantum number ($|m| \leq 2$), which are affected by quantum defects. The later diabatic peak corresponds to the ionization of states with higher m values [$(|m| \geq 2)$], which are interacting much more weakly with the inner electrons (cf. Ref. [28] for more details).

One would expect that with all incident laser beams linearly polarized in the same direction, only states with $m = 0$ shall be excited. However, even small perturbations such as Earth's magnetic field and weak stray electric fields inside the chamber contribute to the population of states with higher m numbers. However, this takes place on a SFI detection time scale which is much larger than the laser-atom interaction times. Thus, the $m > 0$ states play no role in the dynamics under study.

It is in principle possible to analyze the SFI spectra resulting from femtosecond-pulse excitation (upper part of Fig. 3) by fitting the superposition of the peaks corresponding to individual nf states (lower set of individual lines in Fig. 3) by some methods of spectra decomposition and thus obtain a true resolution to individual nf levels (as an example, see Ref. [29] with implementation in the CERN ROOT programming system available). We noticed however that most of the peaks in the SFI spectra of superpositions of nf states excited by the femtosecond pulse result from an equally weighted sum of the signal from the population of two neighboring states; e.g., the sharp peak observed at $t_{\text{SFI}} = 2.8$ μs corresponds to the sum of populations in states $24f$ and $25f$.

It turns out that resolution to following pairs of neighboring levels in fact provides a new additional physical feature which would not be present for the individual levels, as is discussed briefly in the theoretical part and is shown in detail in the first of three reported experiments.

III. THEORY

In our present setup the laser intensity is small enough to apply first-order perturbation theory as an approximate

expression for the amplitudes of the Rydberg nf levels. The first-order expression for a train of identical Gaussian-shaped pulses was calculated by Chen and Yeazell [16]. In the specific case of two pulses with a delay time of $\tau = \Delta t$ between the pulses, the linear polarized electric field in the \hat{z} direction with zero dc component, $\int_0^\infty E(t)dt = 0$, is given as

$$E(t) = E_0 g(\alpha_0, t) \sin(\omega_l t) + E_0 g(\alpha_0, t - \tau) \sin[\omega_l(t - \tau)], \quad (1)$$

where ω_l is the laser frequency, the pulse envelope is $g(\alpha, t) = \exp(-\alpha t^2)$, and $2E_0$ is the maximum field intensity, when $\tau = 0$.

The Rydberg wave function is well described as

$$\Psi(t) = \sum_n a_n(t) \Psi_{n,f}(\vec{r}) e^{-i\varepsilon_n t}, \quad (2)$$

where a_n is the expansion coefficient, $\Psi_{n,f}$ is the stationary f state of the principal level n , and ε_n is the energy. Using the rotating wave approximation, the amplitude for population of each Rydberg n, f state can be written as

$$\begin{aligned} a_n(\tau) &= -\frac{1}{2} E_0 \Omega_n \sqrt{\frac{\pi}{\alpha_0}} e^{-\frac{\Delta_n^2}{4\alpha_0}} (1 + e^{i(\varepsilon_n - \varepsilon_g)\tau}) \\ &= -\frac{1}{2} \Omega_n \tilde{E}_0(\Delta_n) (1 + e^{i(\varepsilon_n - \varepsilon_g)\tau}). \end{aligned} \quad (3)$$

Here Ω_n is the dipole coupling element between the Li(3d) state with energy ε_g and the Rydberg n level and $\Delta_n = \varepsilon_n - \varepsilon_g - \omega_l$. The quantity \tilde{E}_0 is the Fourier transform of the dominant term of the pulse. The resulting probability of excitation of each Rydberg n, f state has a very simple form:

$$P_n(\tau) = |\Omega_n \tilde{E}_0(\Delta_n)|^2 [1 + \cos(\varepsilon_n - \varepsilon_g)\tau] \quad (4)$$

This expression forms the basis of comparisons with experiment in the case of two identical pulses in the following section. The parameter α_0 is extracted from Fig. 2(a).

When the experiment does not resolve the individual n levels, the interference patterns will be superposed. The resulting (unresolved) dependence of the summed total excitation probability on the delay between the pulses has been discussed, e.g., in Ref. [11].

With reference to our experiments we now consider only partial resolution. When adding only two neighboring n -level probabilities obtained from Eq. (3), and approximating the dipole moments to be the same, the two-level-unresolved theoretical signal appears as

$$\begin{aligned} I_{n,n+1} &= |\Omega_n \tilde{E}_0(\Delta_n)|^2 \left\{ 1 + \cos \left[\left(\varepsilon_g - \frac{\varepsilon_n}{2} - \frac{\varepsilon_{n+1}}{2} \right) \Delta t \right] \right. \\ &\quad \left. \times \cos \left[\frac{\varepsilon_n - \varepsilon_{n+1}}{2} \Delta t \right] \right\}. \end{aligned} \quad (5)$$

The shape of Eq. (5), with unrealistic but illustrative values of two adjacent frequencies, is shown in Fig. 4, resembling closely the totally unresolved packet excitation probability given in Fig. 2 of the classical 1992 paper [11]. This interference pattern with beats is the basis of our first experiment discussed in Sec. IV A. The Experiment in Sec. IV B covers the region of time delays which would resolve the fast oscillations but would not be influenced by the envelope pattern observable at much longer delay times. For this case the signal appears as

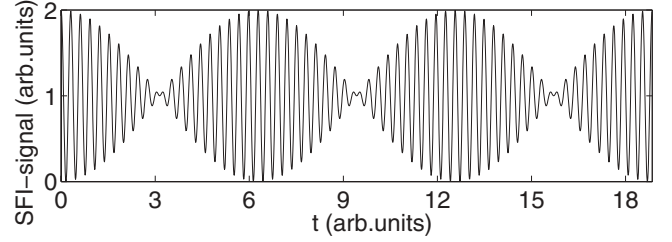


FIG. 4. Plot of the function $0.5[2 + \cos Mt + \cos (M + 1)t]$ of t illustrating the formula Eq. (5) from adding two probabilities of Eq. (4) for the incoherent sum of two interference patterns, here for $M = 20$. The envelope curves $(1 \pm \cos t/2)$ remain the same for all M . Our realistic values would be of the order between $M \approx 900$ and $M \approx 1500$; the faster oscillations would appear to fill the envelope.

a sum of two identical terms and the formula Eq. (4) predicts the interference patterns.

In the case of a chirped second pulse, the expressions for the excitation by two pulses become more complicated due to the phase structure of the chirped pulse. The electric field is now given as

$$E(t) = E_0 g(\alpha_0, t) \sin(\omega_l t) + E_1 g(\alpha_1, t - \tau) \sin[\omega_l(t - \tau) - \Phi(t - \tau)]. \quad (6)$$

The field parameters can again be extracted from Fig. 2. In our setup the phase is quadratic, originating from a linear chirp, $\Phi(x) \approx \Phi_0 + \gamma x^2$ with $x = t - \tau$. Then the second pulse includes the term $\sin[(\omega_l - \gamma x)x - \Phi_0]$, which implies that the higher frequencies arrive first. Performing again the time integral of the first-order perturbation theory gives

$$\begin{aligned} a_n^{\text{lc}}(\tau) &= -\frac{1}{2} E_0 \Omega_n \sqrt{\frac{\pi}{\alpha_0}} e^{-\frac{\Delta_n^2}{4\alpha_0}} \\ &\quad - \frac{1}{2} E_1 \Omega_n e^{i(\varepsilon_n - \varepsilon_g)\tau + \Phi_0} \sqrt{\frac{\pi}{\xi}} e^{-\frac{\Delta_n^2}{4\xi}}, \end{aligned} \quad (7)$$

where $\xi = \alpha_1 - i\gamma$ and the corresponding label “lc” refers to linear chirp. The frequency spectra of the first and second pulse have to be identical; i.e., the absolute value of the Fourier transform of each pulse are the same. Then Eq. (7) can be expressed as

$$a_n^{\text{lc}}(\tau) = -\frac{1}{2} \Omega_n \tilde{E}_0(\Delta_n) \left\{ 1 + e^{i[\phi_0 - \frac{\Delta_n^2}{4\eta} + (\varepsilon_n - \varepsilon_g)\tau]} \right\}, \quad (8)$$

where we have introduced

$$\phi_0 = \arg \left\{ \sqrt{\frac{\pi}{\xi}} e^{i\Phi_0} \right\}, \quad \frac{1}{\eta} = \frac{1}{\alpha_0} \sqrt{\frac{\alpha_0}{\alpha_1} - 1}. \quad (9)$$

This analysis thus shows that the previously well-known oscillatory dependence of Rydberg state amplitudes on the time delay between two successive pulses, given by Eq. (3), is modified in a simple manner when the second pulse is linearly chirped. In this case the interference pattern in τ is modified only by an additional phase, quadratic in the mismatch Δ_n between the main laser frequency and the excitation energy. This phase is state dependent but independent of τ , as is seen in the final result in Eq. (8). It originates from the spectral phase of the chirped pulse, displayed in Fig. 2. We have also established that under the condition of ideal linear chirp there is only one

parameter, which can be chosen as the ratio of the two pulse lengths contained in the ratio $\sqrt{\alpha_0/\alpha_1}$. This additional phase is negative in the case of the down-chirped pulse considered here and is equal but positive for an up-chirped pulse.

IV. RESULTS AND DISCUSSION

Three experiments are presented for three different characters of the pairs of pulses. In all three cases the data collection and analysis are the same, following the description in Sec. II. The SFI spectra are collected for each time delay and placed in a matrix. The SFI spectra are in the form of signal sampled at 1000 values of SFI ramp times. This is repeated for 120 values of time delay in the first case and 60 delay values in the remaining two cases. The raw data of each experiment are thus a 1000×120 or 1000×60 matrix of SFI signal. This matrix is shown as a map in the top part of each of the figures.

The cuts at the values of SFI time indicated in Fig. 3 by vertical lines, corresponding to the contributions from excitation of two adjacent n levels, are shown in the middle panels of the figures. No peak-resolution of the individual n levels is attempted, since in the case of the first experiment this superposition provides new information and the two other cases are kept consistent. The bottom panels of the figures present the theory version of the middle panels given by Eqs. (5) and (4) and scaled to fit the range of the experimental values.

A. Picosecond time delays

In the first part of the experiment we consider time separation between the two-transform-limited pulses on picosecond time scales, i.e., on much longer time scale than required for the Ramsey fringes in Eq. (4). Figure 5 presents the direct SFI spectra of the superposition of Rydberg states. The time delay between pulses has been varied in steps of 0.1 ps. In the Fig. 5(a) the detected SFI voltage depending on the time of the SFI ramp t_{SFI} (y axis) and on the femtosecond pulse delay Δt (x axis) is color coded.

The curves in Fig. 5(b) are obtained by plotting the horizontal cuts from the map in Fig. 5(a) at the SFI times indicated in Fig. 3. The apparent oscillations are the result of sampling the real high frequency oscillation given roughly by Eq. (4) at the measured time delays spaced by 100 fs as compared to the period of real oscillations (2.8 fs for $n = 25$).

Theoretically, adding with equal weight two neighboring n -level probabilities obtained from Eq. (4), and approximating the dipole transition strengths to be the same, the formula Eq. (5) is obtained. This contains the fast optical oscillation with frequency close to the optical frequency of transition from the $3d$ state which in our notation is close to $|\varepsilon_g|$ and a slow modulation with a period close to the so-called classical orbit time $\propto n^3$, i.e., the energy difference between the neighboring n levels. Thus studying the combined population of two neighboring n levels gives the possibility to observe the oscillations with a period of the classical orbit time, by extracting it from the period of the envelopes (cf. Fig. 4). The theoretical orbit times are seen to be in good agreement with the experimental points, falling mainly inside of the theoretical envelope. Equation (5) is displayed in Fig. 5(c).

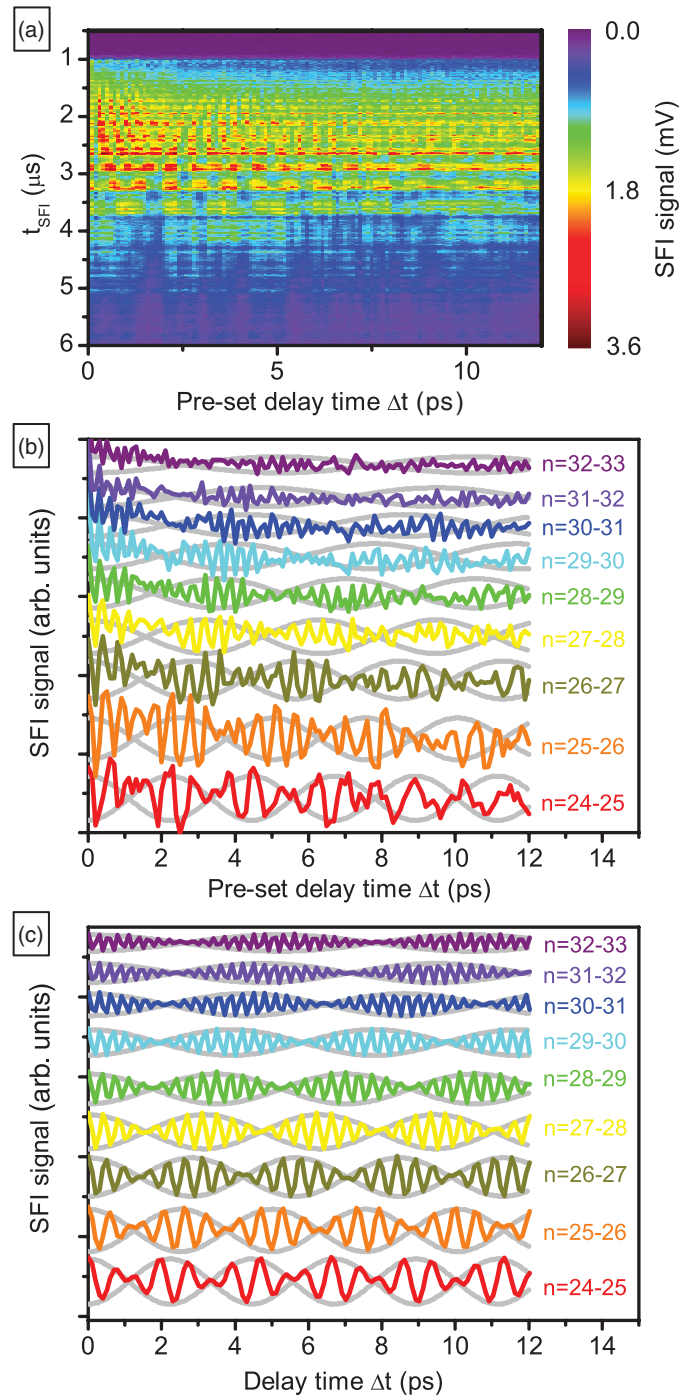


FIG. 5. (Color online) (a) Map of SFI spectra as a function of picosecond scale time delay Δt between two Fourier-transform-limited femtosecond laser pulses. (b) SFI signal from the population of two neighboring nf states (labeled on the right side) as a function of the time delay Δt . Curves were subtracted as horizontal cuts from the map (a) at the SFI times indicated in Fig. 3. Note that the apparent oscillations in panels (b) and (c) are only the result of sampling, the real oscillations are of much higher frequency (cf. Fig. 4). The gray curves are the theoretical envelopes. (c) Theoretical simulation of the population of the pairs of neighboring nf states as a function of time delay Δt between two femtosecond laser pulses. The densely oscillating curve is sampled at the same times as the measured ones. The envelopes (cf. Fig. 4) are plotted in gray and are the same in panels (b) and (c).

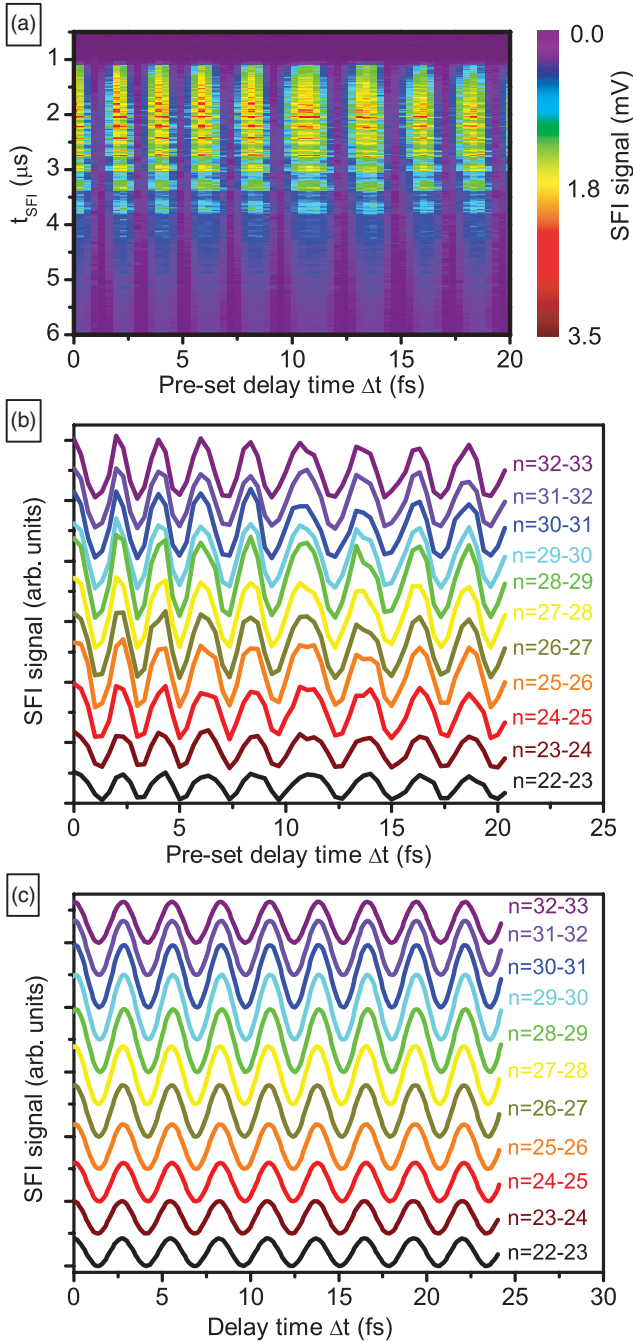


FIG. 6. (Color online) (a) Map of SFI spectra as a function of the femtosecond-scale time delay Δt between two Fourier-transform-limited femtosecond laser pulses. (b) SFI signal from the population of two neighboring nf states (labeled on the right side) as a function of the time delay Δt . Curves were subtracted as horizontal cuts from the map (a) at the SFI times indicated in Fig. 3. (c) Theoretical simulation of evolution of the population of different pairs of neighboring nf states as a function of time delay Δt between the two femtosecond laser pulses. The scale of the time delay is adjusted to reproduce the observed Ramsey interference displayed by in panel (b).

The agreement between the classical orbit times and the experimental and theoretical figures supports the experimental 50%-50% assignment procedure. It also indicates that l mixing due to additional electric fields occurs at time scales larger than the classical orbit time.

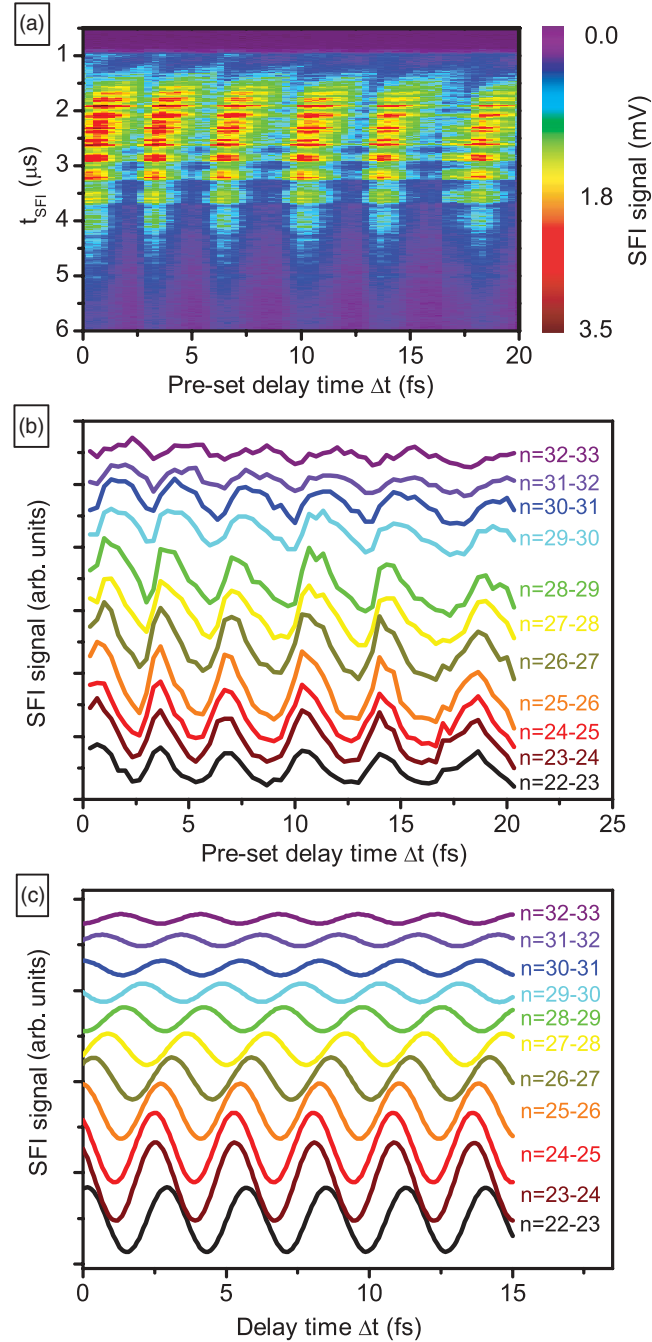


FIG. 7. (Color online) (a) Map of SFI spectra as a function of the femtosecond-scale time delay Δt between one Fourier-transform-limited femtosecond laser pulse and one down-chirped femtosecond laser pulse. (b) SFI signal from the population of two neighboring nf states (labeled on the right side) as a function of the time delay Δt . Curves were subtracted as horizontal cuts from the map (a) at the SFI times indicated in Fig. 3. (c) Theoretical simulation of evolution of the population of different pairs of neighboring nf states as a function of time delay Δt between the two femtosecond laser pulses. The scale of the time delay is adjusted to reproduce the observed Ramsey interference displayed in panel (b).

B. Femtosecond time delays

In the second part of the experiment we study the fast oscillations of the Ramsey fringes which occur at optical

frequencies and are displayed in Fig. 6. The excitation conditions and characters of the displayed subfigures are the same as those for Fig. 5. The main difference is in the time scale, 20 fs in total, and the resolution step, 0.33 fs.

In fact, this experiment corresponds to the refined mesh of the time delay values studied in the first experiment, i.e., in the region where the envelopes appear as horizontal straight lines. Therefore here we should observe the real fast oscillations. With the chosen time delay step the interference fringes should be clearly visible, as is the case in Fig. 6.

In this figure, as well as in Fig. 7, there is a difference between the time delay scale preset by the apparatus and the interferometric time delays following from the theoretical simulation. This experimental phase instability is caused by thermal dilatation of the interferometer arms caused by slight changes in laboratory conditions. Unfortunately, our interferometer was not phase stabilized in a feedback loop, so this instability could not be eliminated. However, this discrepancy is not significant for demonstrating the behavior of the Ramsey fringes in the presented cross-correlation interferograms since a simple rescaling brings the theoretical and experimental results into excellent agreement.

C. Femtosecond time delays with a chirped pulse

In the third part of the experiment we study the cross-correlation interferograms after excitation with a pair of one Fourier-transform-limited pulse and one down-chirped pulse characterized in Fig. 2. Results are shown in Fig. 7. The experimental data are compared with the theoretical Eq. (8) in Fig. 7(c). The parameters of both pulses used in the theoretical calculations were taken from Fig. 2. In general the agreement between theory and experiment is very good. The small discrepancy can be caused by imprecision of evaluation of the exact pulse spectral phase, which is critical in this case. The higher moments of the chirp, caused by the third and higher derivatives of the refractive index, which are not taken into account in the calculation, may also play a role. The negative quadratic phase shift dependence on $\Delta_n^2/4\eta$ is evident in the theoretical as well as the experimental state oscillations.

In Fig. 2 (as in Fig. 6) there is a difference between the time delay scale preset by the apparatus and the interferometric time delays following from the theoretical simulation. This is explained by the thermal instability in the preceding section. Additionally, in Fig. 2(b) for the medium and lower values of n we observe a small additional phase shift of the experimental curves, this is caused by the experimental uncertainty in determining zero time delay, i.e., the simultaneous arrival of the two pulses, caused by the same instability.

The chirped second pulse thus offers an extra adjustable parameter for shaping of the population of the Rydberg states by a pair of femtosecond pulses, where the two identical pulses produce a uniform population for each time delay, whereas one chirped pulse changes the population dramatically. In principle, such pulse pairs also allow the determination of the relative phase between the Rydberg state amplitude at a single selected delay time [18].

V. CONCLUSIONS

In this work we have studied the population of radial Rydberg wave packets in atomic lithium in three different regimes of paired femtosecond laser pulses. Two coherent Fourier-transform-limited pulses were used to excite the n -levels 22–32 delayed at two different time scales. At long delay times, the sum of signals from two neighboring n states due to the combination of two interference patterns results in beats observed as a function of the time delay, reflecting the classical orbit periods of the Rydberg atom.

For delays at short time scales, we observe the fast oscillations in the interference pattern due to the two pulses. The frequencies entering the individual excitation amplitudes of the n components of the wave packet are dominated by the large transition frequency from the $3d$ state and the resulting phases are nearly n independent for the range of femtosecond time delays. This is seen as nearly uniform oscillation of the excitation probabilities.

By chirping one of the pulses the interference pattern changes dramatically. Instead of uniform oscillations, the patterns are phase shifted by a phase quadratically dependent on the distance from the central frequency of the pulse. We have thus demonstrated a possibility of both controlled amplitude and phase manipulation of the created wave packet. This plays a crucial role for the subsequent dynamics, regarding revivals and dispersion or a complex behavior under the addition of further pulses or external fields of the type used in previous types of our experiments (as, e.g., Ref. [26]).

In future experiments we aim at using multiple pulses to increase the diversity in wave packet formation even further.

ACKNOWLEDGMENTS

The authors thank Erik Horsdal for his contribution to the construction of the laboratory facilities in Bergen. This work was supported by The Norwegian Research Council, the Czech Science Foundation (Project No. 202/09/H041), and the EU Seventh Framework Programme under Grant Agreement No. PIRSES-GA-2010-269243.

-
- [1] G. Alber, H. Ritsch, and P. Zoller, *Phys. Rev. A* **34**, 1058 (1986).
 [2] A. ten Wolde, L. D. Noordam, A. Lagendijk, and H. B. van Linden van den Heuvell, *Phys. Rev. Lett.* **61**, 2099 (1988).
 [3] A. ten Wolde, L. D. Noordam, A. Lagendijk, and H. B. van Linden van den Heuvell, *Phys. Rev. A* **40**, 485 (1989).

- [4] L. D. Noordam, A. ten Wolde, A. Lagendijk, and H. B. van Linden van den Heuvell, *Phys. Rev. A* **40**, 6999 (1989).
 [5] J. A. Yeazell, M. Mallalieu, and C. R. Stroud, Jr., *Phys. Rev. Lett.* **64**, 2007 (1990).
 [6] J. A. Yeazell, G. Raithel, L. Marmet, H. Held, and H. Walther, *Phys. Rev. Lett.* **70**, 2884 (1993).

- [7] J. F. Christian, B. Broers, J. H. Hoogenraad, W. J. van der Zande, and L. D. Noordam, *Opt. Commun.* **103**, 79 (1993).
- [8] B. Broers, J. F. Christian, J. H. Hoogenraad, W. J. van der Zande, H. B. van Linden van den Heuvell, and L. D. Noordam, *Phys. Rev. Lett.* **71**, 344 (1993).
- [9] J. Wals, H. H. Fielding, J. F. Christian, L. C. Snoek, W. J. van der Zande, and H. B. van Linden van den Heuvell, *Phys. Rev. Lett.* **72**, 3783 (1994).
- [10] B. Broers, J. F. Christian, and H. B. van Linden van den Heuvell, *Phys. Rev. A* **49**, 2498 (1994).
- [11] L. D. Noordam, D. I. Duncan, and T. F. Gallagher, *Phys. Rev. A* **45**, 4734 (1992).
- [12] R. R. Jones, C. S. Raman, D. W. Schumacher, and P. H. Bucksbaum, *Phys. Rev. Lett.* **71**, 2575 (1993).
- [13] M. W. Noel and C. R. Stroud, Jr., *Phys. Rev. Lett.* **75**, 1252 (1995).
- [14] M. W. Noel and C. R. Stroud, Jr., *Phys. Rev. Lett.* **77**, 1913 (1996).
- [15] J. F. Christian and B. Broers, *Phys. Rev. A* **52**, 3655 (1995).
- [16] X. Chen and J. A. Yeazell, *Phys. Rev. A* **55**, 3264 (1997).
- [17] M. W. Noel and C. R. Stroud, Jr., *Opt. Express* **1**, 176 (1997).
- [18] R. R. Jones and M. B. Campbell, *Phys. Rev. A* **61**, 013403 (1999).
- [19] X. Zhang and R. R. Jones, *New J. Phys.* **11**, 105050 (2009).
- [20] D. W. Schumacher, J. H. Hoogenraad, D. Pinkos, and P. H. Bucksbaum, *Phys. Rev. A* **52**, 4719 (1995).
- [21] T. C. Weinacht, J. Ahn, and P. H. Bucksbaum, *Phys. Rev. Lett.* **80**, 5508 (1998).
- [22] T. C. Weinacht, J. Ahn, and P. H. Bucksbaum, *Nature (London)* **397**, 233 (1999).
- [23] J. Ahn, T. C. Weinacht, and P. H. Bucksbaum, *Science* **287**, 463 (2000).
- [24] R. E. Carley, E. D. Boléat, R. S. Minns, R. Patel, and H. H. Fielding, *J. Phys. B* **38**, 1907 (2005).
- [25] W. L. Fugua and K. B. MacAdam, *Rev. Sci. Instrum.* **56**, 385 (1985).
- [26] A. Waheed, D. Fregenal, Ø. Frette, M. Førre, B. T. Hjertaker, E. Horsdal, I. Pilskog, and J. Preclikova, *Phys. Rev. A* **83**, 063421 (2011).
- [27] J. Preclíková, A. Waheed, D. Fregenal, Ø. Frette, B. Hamre, B. T. Hjertaker, E. Horsdal, I. Pilskog, and M. Førre, *Phys. Rev. A* **85**, 043416 (2012).
- [28] T. F. Gallagher, *Rydberg Atoms* (Cambridge University, New York, 1994).
- [29] M. Morhac, J. Kliman, M. Jandel, L. Krupa, and V. Matousek, *Appl. Spectrosc.* **57**, 753 (2003).